Int J Fract
DOI 10.1007/s10704-010-9479-4

ORIGINAL PAPER

Pulse-like and crack-like dynamic shear ruptures on frictional interfaces: experimental evidence, numerical modeling, and implications

Xiao Lu · Nadia Lapusta · Ares J. Rosakis

Received: 16 November 2009 / Accepted: 11 March 2010
© Springer Science+Business Media B.V. 2010

Abstract Destructive large earthquakes occur as dynamic frictional ruptures along pre-existing interfaces (or faults) in the Earth's crust. One of the important issues in earthquake dynamics is the local duration of relative displacement or slip. Seismic inversions show that earthquakes may propagate as self-healing pulse-like ruptures, with local slip duration being much shorter than the overall rupture duration. Yet many classical models produce crack-like ruptures, with local slip durations comparable to the overall rupture duration. We study rupture modes in an experimental set up designed to mimic a fault prestressed both in compression and in shear. Our experiments demonstrate systematic variation from crack-like to pulse-like rupture modes as nondimensional shear prestress is decreased. The results of our experiments are consistent with theories of ruptures on interfaces with velocity-weakening friction. To consider the possibility that slip-weakening friction can also result in such rupture mode transition in the presence of the dynamic nucleation procedure employed by the experimental setup, we conduct numerical simulations with linear slip-weakening friction. In the simulations, we use the parameter regimes that were shown in previous studies to reproduce supershear transition distances obtained in the same experimental setup. We find that simulations with linear slip-weakening friction are unable to reproduce pulse-like ruptures, even in the presence of the dynamic initiation procedure. Our experimental results and simulations imply that velocity-weakening friction plays an important role in dynamic behavior of shear ruptures and needs to be included in earthquake models.

Keywords Earthquake physics · Mechanics of faulting · Pulse-like rupture · Shear cracks · Velocity-dependent friction · Linear slip-weakening friction

X. Lu · A. J. Rosakis
Graduate Aerospace Laboratories, California Institute of Technology, Pasadena, CA 91125, USA

X. Lu
e-mail: xiaolu.galcit@gmail.com

A. J. Rosakis
e-mail: rosakis@aero.caltech.edu

N. Lapusta (✉)
Division of Engineering and Applied Science and Division of Geological and Planetary Sciences, California Institute of Technology, Pasadena, CA 91125, USA
e-mail: lapusta@its.caltech.edu

1 Introduction

Destructive large earthquakes occur as dynamic frictional ruptures along pre-existing interfaces (or faults) in the Earth's crust. Inversions of seismic and other field observations have significantly advanced our understanding of earthquake ruptures. However, inversions

Published online: 20 April 2010

are often non-unique and lack detail due to limited data availability and limited knowledge of the structure and properties of the crust. This reality highlights the need for combined experimental and theoretical studies that both record dynamic rupture phenomena in highly-instrumented experiments and analyze the experimental findings through numerical models to understand implications for fault friction and rupture dynamics.

Numerical models of shear frictional ruptures often use linear slip-weakening friction (e.g., Andrews 1976; Das and Aki 1977; Day 1982; Archuleta 1984; Madariaga and Olsen 2000; Uenishi and Rice 2003; Festa and Vilotte 2006; Liu and Lapusta 2008; Lu et al. 2009) proposed by analogy with cohesive zone models of tensile fracture (Ida 1972). This simplified friction model is convenient, easy to implement, produces results that can be compared to classical theoretical developments, and captures one of the essential features of frictional resistance that leads to dynamic rupture, namely the decrease of friction during sliding. However, accumulating experimental, observational, and theoretical findings suggest that friction is intrinsically dependent on slip velocity. Friction laws formulated based on laboratory experiments and theories of frictional resistance combine velocity dependence of friction with transient slip-dependent effects (e.g., Dieterich 1979, 2007, 1981; Ruina 1983; Rice 2006; Tullis 2007; Noda et al. 2009).

One issue that can help determine whether the linear slip-weakening formulation of friction is adequate for reproducing all basic rupture phenomena, or whether inclusion of velocity-dependent features is necessary, is that of pulse-like vs. crack-like rupture modes. Early models of dynamic shear rupture considered the crack-like mode of earthquake propagation, in which the duration of slip at each point on the fault is comparable to the overall rupture duration (Kostrov 1966; Ida 1972; Andrews 1976; Madariaga 1976). However, seismic inversions indicate (Kanamori and Anderson 1975; Heaton 1990) that ruptures on real faults may propagate in the pulse-like mode, in which slip duration at a point is much shorter than the overall rupture duration. Theoretical and numerical studies have shown that the issue of rupture modes may have important implications for fault constitutive laws, stress conditions on faults, energy partition and heat generation during earthquakes, scaling laws, and spatio-temporal complexity of slip (e.g., Heaton 1990; Cochard and Madariaga 1994, 1996; Perrin et al. 1995; Beeler and Tullis 1996; Zheng and Rice 1998; Nielsen et al. 2000; Ben-Zion 2001; Nielsen and Madariaga 2003; Shi et al. 2008; Noda et al. 2009).

Pulse-like ruptures have been obtained in a number of numerical simulations that include significant weakening of interface friction with sliding velocity (Cochard and Madariaga 1994, 1996; Perrin et al. 1995; Beeler and Tullis 1996; Zheng and Rice 1998; Nielsen et al. 2000; Lapusta and Rice 2004; Shi et al. 2008). This implies that fault friction may be characterized by significant velocity weakening, a conclusion further supported by a number of recent rock experiments and theoretical studies that have uncovered strongly velocity-weakening friction at seismic slip velocities (e.g., Tsutsumi and Shimamoto 1997; Tullis and Goldsby 2003; Di Toro et al. 2004; Yuan and Prakash 2008a,b; Rice 2006; Tullis 2007). Other explanations for the occurrence of pulse-like ruptures include interaction of rupture with fault geometry or local heterogeneities (e.g., Day 1982; Johnson 1992; Beroza and Mikumo 1996; Olsen et al. 1997; Day et al. 1998) and normal stress variation due to difference in material properties across the interface (bi-material effect) (e.g., Andrews and Ben-Zion 1997; Cochard and Rice 2000; Ben-Zion 2001). Which mechanism dominates in real earthquakes remains an open research question.

Both pulse-like and crack-like ruptures have been produced in the laboratory. The first experiments with pulse-like sliding were done with strong impact loading and interfaces with no shear prestress (Lykotrafitis et al. 2006a). However, those loading conditions are quite different from the ones on tectonically loaded faults in the Earth's crust. The work of Lu et al. (2007, 2010) was the first to obtain pulse-like ruptures in a configuration that contains an interface prestressed both in compression and in shear, similar to natural faults that host earthquakes. The experimental setup was adopted from that of supershear rupture studies (Rosakis 2002; Xia et al. 2004; Rosakis et al. 2007) and included experimental diagnostics that allowed to conclusively determine the mode and speed of rupture propagation (Rosakis 2002; Lykotrafitis et al. 2006a).

We present experimental results on systematic variation from crack-like to pulse-like rupture modes with fault prestress in Sect. 2. The geometry, loading, and nucleation mechanism in the experiments

are essentially two-dimensional (2D). This configuration is relevant for understanding the dynamics of large strike-slip earthquakes which are dominated by in-plane sliding. The configuration constitutes an experimental equivalent of 2D in-plane or Mode II numerical models of dynamic rupture which are common in earthquake studies (Andrews 1976; Das and Aki 1977; Beeler and Tullis 1996; Andrews and Ben-Zion 1997; Cochard and Rice 2000; Ben-Zion 2001; Festa and Vilotte 2006; Shi and Ben-Zion 2006; Liu and Lapusta 2008; Shi et al. 2008).

The existence of pulses in the experimental configuration with no bi-material effect and no local heterogeneities points to the importance of velocity-weakening friction in rupture dynamics. This conclusion is further strengthened by the consistency of experimental observations with theories of ruptures on velocity-weakening interfaces (Zheng and Rice 1998; Samudrala et al. 2002; Lu et al. 2007, 2010). However, those considerations do not take into account the nucleation procedure. Recent studies (Festa and Vilotte 2006; Shi and Ben-Zion 2006; Liu and Lapusta 2008; Shi et al. 2008; Lu et al. 2009) have shown that rupture initiation procedure can affect the characteristics of propagating rupture, including the rupture mode. In the experiments, rupture is initiated by a wire explosion that may be interpreted as local decrease of compression (Lu et al. 2010).

That is why, in Sect. 3, we explore whether the existence of pulse-like ruptures and the systematic variation of rupture modes with fault prestress can be explained by the combination of the rupture initiation procedure and linear slip-weakening friction. We use the same model as in Lu et al. (2009) who successfully used it to match the experimentally observed supershear transition distances of Xia et al. (2004). Lu et al. (2009) identified two parameter regimes, in terms of friction parameters and parameters of the nucleation procedure that can match the supershear experiments. We explore both of those parameters regimes and find that, even in the presence of the dynamic initiation procedure, the simulations with linear slip-weakening friction cannot produce pulse-like ruptures presented in Sect. 2. Rather, simulations with linear slip-weakening result in ruptures dying right outside the nucleation region for prestress levels that correspond to pulses in the experiments. This further amplifies the importance of using velocity-dependent friction laws, as discussed in the concluding Sect. 4.

2 Experimental results

2.1 Experimental set up that mimics crustal earthquakes

Our experimental setup mimics a fault in the Earth's crust prestressed both in compression and in shear (Xia et al. 2004; Lu et al. 2007, 2010; Rosakis et al. 2007). A square Homalite plate, with the dimensions 150 mm × 150 mm × 10 mm, is cut to introduce an interface with an inclination angle α with respect to the horizontal (Fig. 1). Unidirectional compression P is applied to the top and bottom edges. The interface surfaces are treated to create the same texture and hence the same friction properties in all specimens (Lu et al. 2010). Elastic properties of the bulk material, Homalite, are well documented (Dally and Riley 1991): Young's modulus $E = 3.86$ GPa, shear modulus $\mu = 1.43$ GPa, Poisson's ratio $\nu = 0.35$, density $\rho = 1200$ kg/m^3, shear wave speed $C_s = 1249$ m/s, longitudinal wave speed $C_p = 2187$ m/s, and Rayleigh wave speed $C_R = 1155$ m/s.

Dynamic rupture is initiated in the middle of the plate by an explosion of a thin wire. A nickel wire with a diameter of 0.08 mm is embedded within a 0.1-mm hole across the entire plate thickness. The ends of the wire are connected to a charged capacitor. By abrupt discharge, the stored electric energy is released and the surge of the current turns the wire into plasma (Rosakis et al. 2007). The explosion relieves fault-normal compression locally, decreasing friction and allowing shear rupture to start under the action of the resolved shear stress in a region around the explosion site. Afterwards, dynamic rupture propagates spontaneously outside the nucleation region. The nucleation mechanism of the wire explosion has multiple experimental advantages. It allows us to synchronize diagnostic instruments, to start dynamic rupture with known and adjustable stress conditions outside of the nucleation region, and to reproduce the same experimental conditions multiple times while taking different diagnostic measurements. At the same time, the initiation procedure introduces additional complexity. To evaluate its effect on the resulting dynamic ruptures, we have conducted experiments with explosions of different strength and found that local slip durations and hence rupture modes are independent the explosion strength (Lu et al. 2010). Normal stress changes outside of the nucleation region were evaluated by performing

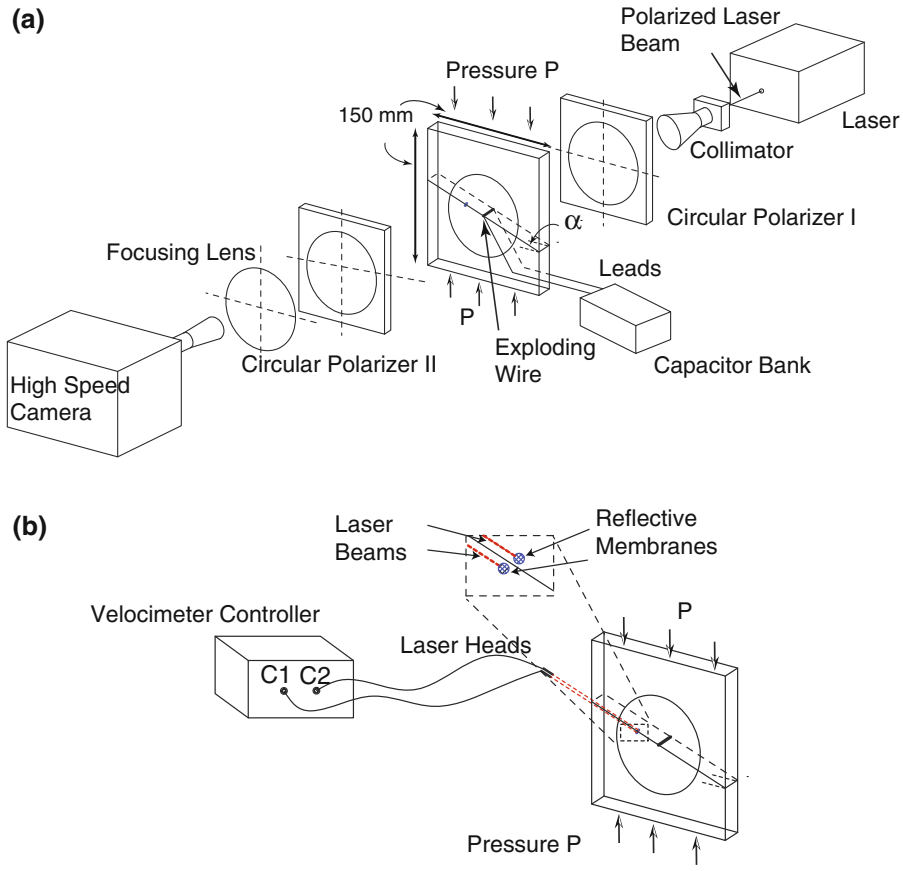

Fig. 1 Schematic illustration of the experimental configuration. **a** A Homalite sample is cut to introduce an interface with an inclination angle α and compressed with the load P. Dynamic photoelasticity is used to capture the full-field information of rupture propagation. Rupture nucleation is achieved by a local pressure release due to an explosion of a thin wire. **b** Laser velocimetry is used to capture the local sliding velocity of the interface

fault-normal velocity measurements (Lu et al. 2010), with the conclusion that there is no significant normal stress change induced by the nucleation procedure outside of the nucleation region.

Dynamic rupture propagation is captured using high-resolution dynamic photoelasticity and laser velocimetry (Lykotrafitis et al. 2006a,b; Rosakis et al. 2007). The bilaterally spreading rupture is observed only until reflected waves return from the edges of the plate, to enable comparisons with 2D models of dynamic rupture in infinite elastic media. A typical observation window is 65 μs. In addition to the full-field photoelastic images (Fig. 1a), we use two velocimeters based on laser interferometry to measure particle velocity histories of two points, one above and one below the fault interface (Fig. 1b). Two reflective membranes are glued at the points of interest, and two separate laser beams are focused on the sides of the two membranes to record either the fault-parallel or fault-normal particle velocity. The difference between the two measured fault-parallel particle velocities represents the interface sliding velocity plus elastic deformation between the two measurement points (Rosakis et al. 2007). The elastic deformation is taken into account when the onset and healing of the interfacial sliding is determined (Lu et al. 2007, 2010). The velocimeters have the maximum frequency response of 1.5 MHz and can measure particle velocity of up to 10 m/s, enabling us to record rapidly varying high slip velocity at rupture fronts.

2.2 Systematic variation of rupture mode from crack-like to pulse-like with nondimensional shear prestress

Experimental parameters P and α determine the resolved shear traction $\tau_0 = P \sin\alpha \cos\alpha$ and normal traction $\sigma_0 = P \cos^2\alpha$ on the interface. The nondimensional shear prestress $f_0 = \tau_0/\sigma_0 = \tan\alpha$ indicates how close the interface is to static failure according to the Coulomb criterion. Because the static friction

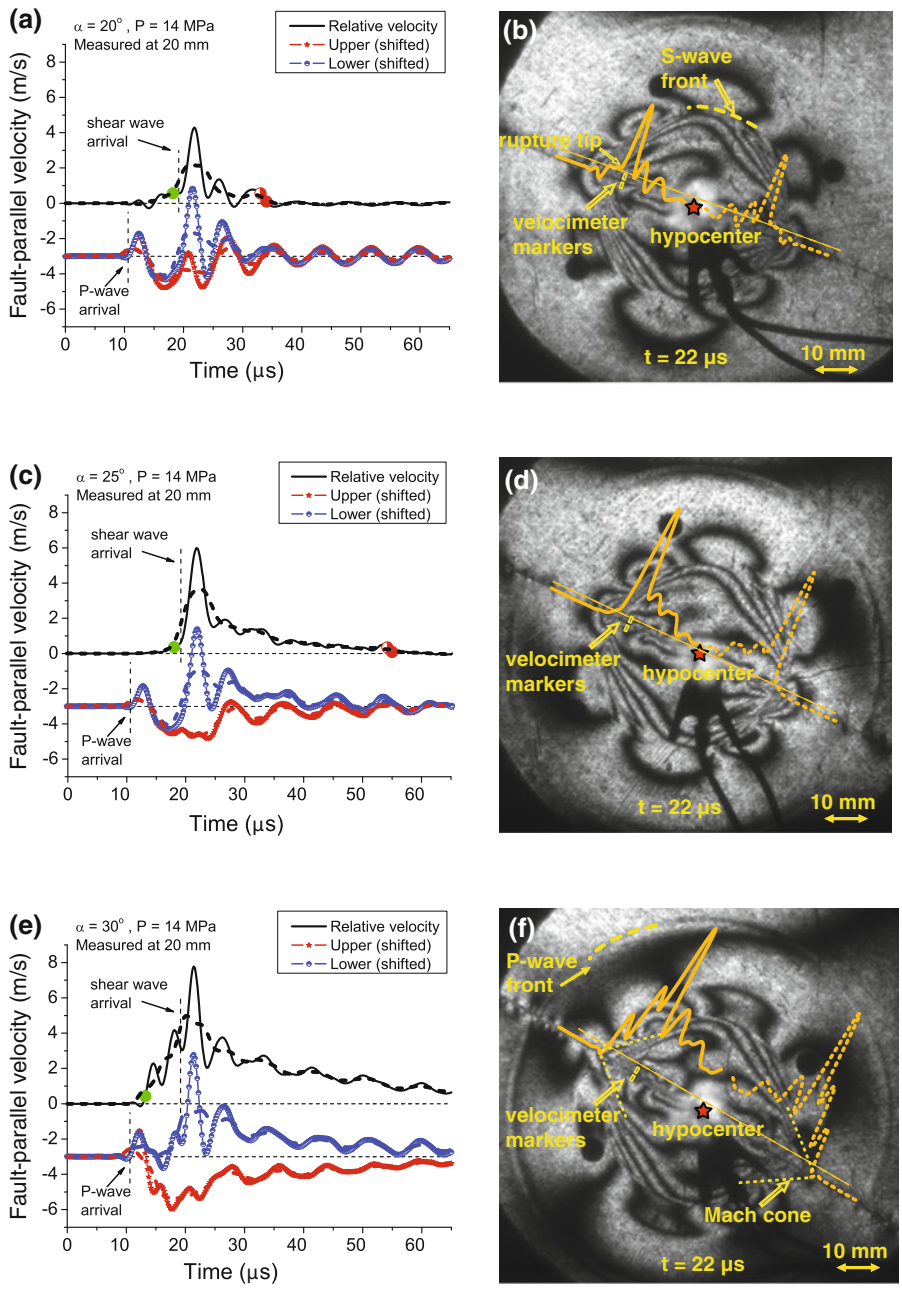

Fig. 2 Variation of rupture modes with the interface inclination angle in the experiments. **a, c, e** Measurements of particle velocities above (*blue lines marked with circles*) and below (*red lines marked with stars*) the interface at the location of 20 mm from the rupture initiation, shifted by −3 m/s for clarity. Their difference is shown in *black solid lines*. The rupture mode systematically varies from pulse-like in (*a*) to crack-like in (*e*). **b, d, f** The corresponding full-field photoelastic images. *Markings* and *lines* are explained in the main text

coefficient of the interface is about 0.6, the inclination angle α is chosen to be 30° or smaller to ensure that sliding does not occur during the static preloading stage.

To study the dependence of dynamic rupture on interface prestress, we conduct experiments with the decreasing inclination angle α, starting from $\alpha = 30°$ that corresponds to the nondimentional shear prestress $f_0 = \tau_0/\sigma_0 = \tan\alpha = 0.58$. As angle α decreases, so does the nondimensional shear prestress, making the rupture propagation more difficult. We find that the rupture responds by adjusting the rupture mode from crack-like for $\alpha = 30°$ to pulse-like for $\alpha = 25°$ and $\alpha = 20°$ (Fig. 2). Note that this is not a trivial result, as an alternative possibility would be to have, for lower prestress values, no rupture propagation at all.

Indeed, as we will see in Sect. 3, simulations with linear slip-weakening friction predict no rupture for angles between about $\alpha = 25°$ and $\alpha = 20°$.

Let us consider the experimental results in more detail. Figure 2 presents velocimeter measurements in the left column and photoelastic images in the right column for three experiments with inclination angles $\alpha = 20°$ (top row), $\alpha = 25°$ (middle row), and $\alpha = 30°$ (bottom row). Particle velocities and their relative values shown in the left column are measured at the location of 20 mm from the rupture initiation. Individual channels marked as "upper" and "lower" correspond to particle velocity histories of points above and below the interface, respectively; the plotted measurements are shifted by −3 m/s for clarity. The oscillations in the individual channels are related to the plate thickness, as demonstrated by Lu et al. (2010) by considering plates of different thickness. To approximately remove this 3D effect, we plot smoothed velocity profiles that are constructed by averaging the measurements within the window of 5 μs (dashed lines in the left column of Fig. 2). These dashed lines point to approximately anti-symmetric behavior, as would be expected for shear rupture. Deviations from anti-symmetry and potential reasons for it are discussed in Lu et al. (2010).

For all three cases, the points on the two sides of the interface start to move shortly after 10 μs when the P-wave arrives. They move together initially and then exhibit relative motion. The relative motion is the sum of the elastic deformation between the two points and relative sliding, or slip, on the interface. Relative velocity between the two measurement points is computed by subtracting the velocity history of the point below the interface from that above the interface. Green dots indicate our estimate of rupture arrival time or the initiation of relative sliding at the location of 20 mm. To determine the onset of interface slip, we compute the relative displacement between the two measurement locations and take the slip onset to correspond to the value of displacement that would make the shear stress between the measurement locations equal to the static friction strength, assuming uniform shear between the two points (Lu et al. 2007, 2010). After rupture initiation, the relative velocity reaches the maximum of 5–8 m/s, depending on the fault prestress.

For $\alpha = 30°$, the relative velocity is of the order of 1 m/s throughout the observation window. This means that the interface does not lock during the observation window, indicating what we define to be a crack-like mode. For $\alpha = 25°$ and $\alpha = 20°$, the relative velocity decreases to near-zero values within the observation window, pointing to pulse-like rupture. Note that the interface can be locked while the relative velocity has small non-zero values, due to elastic deformation between the measurement locations and to small experimental errors that can result from slight deviations in beam alignment and other factors. To estimate the interface locking time, we use two criteria (Lu et al. 2007, 2010). According to the first criterion, sliding stops when the relative velocity becomes smaller than the elastic cut-off value $\dot{\delta}_c$. If the relative velocity decreases below $\dot{\delta}_c$ several times, we take the last time as the time of interface locking. Those times are marked by half-filled red dots in Fig. 2. The second, more conservative, criterion is to insist that the relative velocity drops to zero and that the integral of relative velocity from that time until the end of observation time is a small fraction (<5%) of the total accumulated relative displacement. The corresponding times are marked by fully filled red dots in Fig. 2. As Fig. 2 shows, the two locking criteria produce very similar results with respect to rupture duration and hence rupture mode identification.

The timing of the shear wave arrival, indicated by a vertical dashed line on the relative velocity trace, provides us with a way of judging whether rupture is supershear at the location of 20 mm or not. For $\alpha = 30°$ (Fig. 2e), it is apparent that the rupture is supershear, as it arrives much sooner than the shear wave. In the other two cases (Fig. 2a, c), the rupture arrival and shear wave arrival approximately coincide. Note that both the rupture arrival time and the shear wave arrival time are indicated with some assumptions. The criterion for the rupture arrival includes assumptions on how much relative displacement can occur elastically between the measurement locations. The shear wave arrival time is marked assuming that shear waves are emitted at the time of the capacitor discharge, but heating and explosion of the wire can take some time. Hence the position of the green dot in Fig. 2a, b could be right behind the shear wave arrival instead of right in front of it, and all we can conclude is that the rupture speed is approximately equal to the shear wave speed, although it could be sub-Rayleigh. That is why we need to use photoelastic images that show the development of the rupture along the interface to conclusively determine the rupture speed.

To visualize rupture propagation, the relative velocity records are superimposed on the photoelastic field

images (the right column of Fig. 2). The photoelastic snapshots shown are taken 22 μs after the wire explosion. They are the closest images in time to the shear wave arrival at the location of the velocimeter measurements. The superposition of velocimeter measurements and photoelastic images converts time-dependent rupture history at one location into an approximation of the space-dependent rupture profile at the time of the photoelastic snapshot. Converting the time history of the sliding velocity into spatial variation along the fault is based on the assumption of a constant rupture speed. Since rupture is expected to be equi-bilateral, a mirrored profile (with respect to the nucleation site) is added for visualization purposes. The hypocenter is marked by a star. The circular P-wave and S-wave fronts are marked with dashed lines. We see that the arrivals of rupture tips are associated with high fringe density that marks stress concentrations. For $\alpha = 30°$, the Mach cones are beginning to form, consistent with the velocimeter measurements that point to supershear rupture arrival at the location of 20 mm.

For each experiment, we have a set of 16 photoelastic images that allows us to compute the evolution of rupture speed as the rupture propagates along the interface (Lu et al. 2010). Based on the combined diagnostics of laser velocimetry and dynamic photoelasticity, we can confirm that rupture in the case of $\alpha = 30°$ is indeed supershear, at the location of 20 mm and during subsequent propagation. In the case of $\alpha = 25°$, rupture becomes supershear within the experimental window of observation, with the location of 20 mm being close to the location of supershear transition. For $\alpha = 20°$, rupture stays subshear throughout the observation window. Hence we have a supershear pulse for $\alpha = 25°$ and sub-Rayleigh pulse for $\alpha = 20°$.

Figure 3 compares the relative displacements at the location of 20 mm for the three experimental cases. The crack-like rupture in the case of $\alpha = 30°$ has the largest displacement that would likely increase further if our observation window was longer. The pulse-like ruptures have smaller relative displacements which level off before the end of the observation window. The Figure also clearly shows the progressive decrease in local rupture duration for smaller angles and hence lower nondimensional shear prestress level.

The rupture modes observed in our experiments are summarized in Fig. 4. The results presented in Figs. 2, 3 correspond to the compressive load of

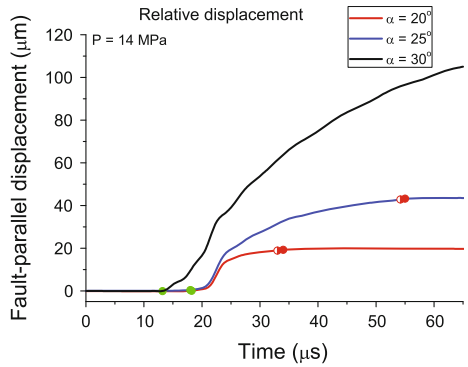

Fig. 3 The relative displacement between two velocimeter measurement locations for the three cases of Fig. 2. For pulse-like ruptures (red line of 20° case, and blue line of 25° case), accumulation of the relative displacement stops within the window of observation. For the crack-like rupture, the relative displacement continues to increase. *Green* and *red dots* indicate our estimates of the rupture initiation and arrest on the interface, respectively, as discussed in the main text

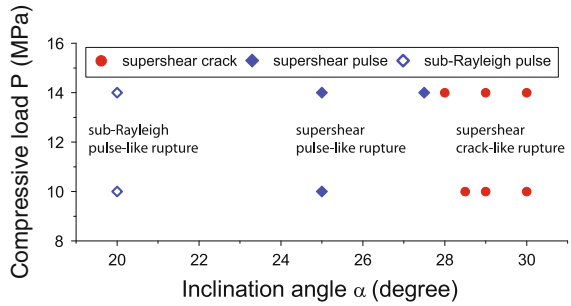

Fig. 4 Rupture modes in experiments with different experimental conditions. The experimental results show clear variation from sub-Rayleigh pulse-like ruptures to supershear pulse-like ruptures to supershear crack-like ruptures as the inclination angle is increased, for two values of the compressive load. Experimental results for higher compressive loads are given in Lu et al. (2010)

14 MPa. Figure 4 also show the rupture modes for the case of 10 MPa, to demonstrate that the results are not restricted to one value of the compressive load. Note that, for most experimental conditions, multiple experiments were conducted to verify the rupture mode and speed. Figure 4 shows a clear systematic variation from sub-Rayleigh pulse-like ruptures to supershear crack-like ruptures as the inclination angle or, equivalently, the nondimentional shear prestress, is increased. We will use this diagram to compare the experimental results with the results of numerical simulations presented in Sect. 3. Rupture modes for a wider range of compressive loads P were reported in Lu et al. (2010).

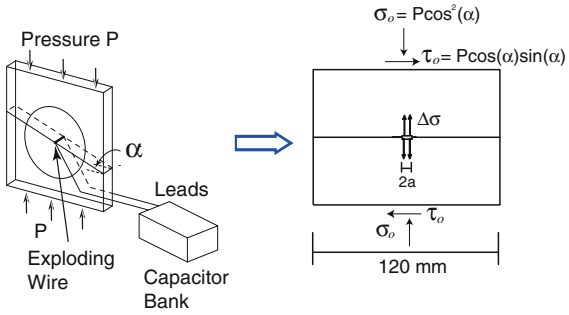

Fig. 5 Model that mimics the experimental set up. We consider a planar interface embedded into a uniform isotropic elastic medium under plane stress conditions, as appropriate for a thin plate. The interface is prestressed both in compression, with $\sigma_0 = P\cos^2\alpha$, and in shear, with $\tau_0 = P\sin\alpha\cos\alpha$. The rupture is initiated by applying a transient reduction $\Delta\sigma$ of normal stress in the region of length $2a$ in the middle of the interface, as illustrated in Fig. 6

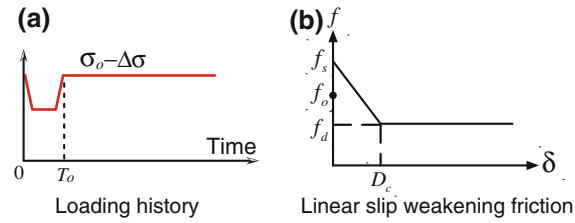

Fig. 6 **a** Time dependence of the normal stress reduction assumed in the nucleation region. **b** Linear slip-weakening friction. In the model, the static coefficient is set to $f_s = 0.6$. Two sets of values for the dynamic friction coefficient f_d and critical slip D_c are considered, based on the study of Lu et al. (2009)

3 Modeling experiments with slip-weakening friction

3.1 Model with dynamic rupture initiation procedure

As explained in the introduction, we would like to explore whether the systematic variation of rupture modes with fault prestress presented in Sect. 2 can be captured by a model that incorporates an interface governed by linear slip-weakening friction and a dynamic rupture initiation procedure that mimics the effect of the wire explosion used in the experiments.

We adopt the model used by Lu et al. (2009) to numerically simulate and match supershear transition distances observed by Xia et al. (2004). In the model, a planar interface is embedded into a uniform isotropic elastic medium with Homalite properties in the context of a two-dimensional plane-stress problem. The interface is prestressed with shear and normal stresses $\tau_0 = P\sin\alpha\cos\alpha$ and $\sigma_0 = P\cos^2\alpha$, respectively, where P and α are the parameters of the experiment we would like to model (Fig. 5).

The rupture initiation procedure adopted in the model (Figs. 5, 6a) is intended to capture the dynamic nature of the wire explosion. While the wire is less than 0.1 mm thick, it turns into plasma due to the electric current surge, and hence it can affect a larger region along the interface than the 0.1-mm thickness would suggest. After each experiment, the interface surfaces contain a thin layer of metallic particles around the explosion site. The spatial extent of the layer is typically 4–10 mm along the interface. We model the effect of the plasma by applying a reduction $\Delta\sigma$ of normal stress over a region of size $2a$. For simplicity, we keep the normal stress reduction uniform over that region. The duration of the normal-stress reduction is $T_o = 5$ μs, consistently with the estimates of Rosakis et al. (2007) and the preferred value in Lu et al. (2009). Normal stress is reduced by $\Delta\sigma$ linearly over 1 μs, kept at the level $(\sigma_0 - \Delta\sigma)$ for 3 μs, and then brought back to the original level linearly over 1 μs (Fig. 6a). The normal-stress variation reduces the frictional strength of the interface and allows the sliding to initiate and develop under the applied shear stress. Note that the normal-stress reduction $\Delta\sigma$ we use in the model is always smaller than the applied normal stress σ_0 so that there is no interface opening. In the experiments, the wire explosion might cause local opening of the interface; investigating such scenarios is a goal for future research.

The interface friction is modeled as linear slip-weakening friction with the static friction coefficient f_s, dynamic friction coefficient f_d, and critical slip D_c (Fig. 6b). The static friction coefficient for our experimental interfaces is well-constrained as $f_s = 0.6$, a typical value for many materials including rocks. For the other friction parameters and for the rupture initiation procedure, we use values from the two regimes identified by Lu et al. (2009) as the ones that allowed to match the supershear transition distances experimentally observed by Xia et al. (2004). In the first parameter regime, $f_d = 0.2$, $D_c = 13$μm, $a = 5$ mm, and $\Delta\sigma = 5$ MPa. In the second parameter regime, $f_d = 0.34$, $D_c = 1$ μm, $a = 0.8$ mm, and $\Delta\sigma = 3$ MPa. As explained in Lu et al. (2009), there is a trade-off between the values of f_d and D_c in matching the supershear transition distances, with the two parameter

regimes bracketing what is reasonable in terms of the dynamic friction coefficient and the resulting critical crack sizes.

The numerical simulations in this work are performed using a spectral boundary-integral method (Geubelle and Rice 1995; Liu and Lapusta 2008). The elastodynamic response of the surrounding medium is expressed as an integral relationship between stress and slip on the interface. We use the numerical implementation of the boundary-integral method of Liu and Lapusta (2008). In our model, the interface is discretized uniformly with such a grid that the ratio of the critical crack half length L_c and cell size h is more than 50 for all calculations. In some cases, higher resolution is used to validate the numerical convergence. The cohesive zone size is well-resolved in all simulations.

3.2 Inability of the model to produce pulse-like ruptures

We conduct numerical simulations for the range of experimental parameters of Fig. 4 that shows the systematic variation from crack-like to pulse-like modes. Two levels of compressive load, $P = 10$ MPa and $P = 14$ MPa, and a number of inclination angles from 20 to 30° are simulated. The map of rupture modes obtained in the simulations is given in Fig. 7. For the first parameter regime (Fig. 7a), there are only two distinct rupture modes: supershear crack-like rupture and no rupture. For the second parameter regime (Fig. 7b), sub-Rayleigh crack-like ruptures are also observed. None of the simulations produce pulse-like ruptures. As the inclination angle α, and hence the nondimensional interface prestress $f_0 = \tau_0/\sigma_0 = \tan\alpha$, is decreased, the simulated rupture mode abruptly changes from crack-like rupture to no rupture propagation outside of the nucleation region. The boundary is schematically marked by a dashed line in Fig. 7a, b. Such behavior is clearly inconsistent with experimental results.

Figure 8 illustrates rupture development for two representative cases right next to the separating dashed line, as marked by small squares in Fig. 7a. The corresponding inclination angles are 23.5 and 24°, and the equivalent nondimensional prestress levels are 0.44 and 0.45, respectively. Snapshots of the relative velocity of the two sides of the interface, also called slip velocity, are shown for 4, 12, and 20 μs. For both cases, the

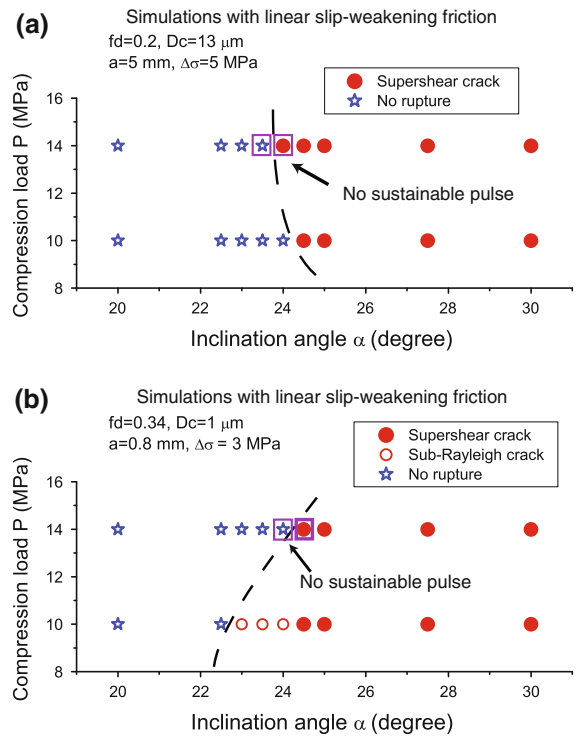

Fig. 7 Numerical simulations with linear slip-weakening friction that reproduce the range of experimental parameters shown in Fig. 4. The simulations produce either crack-like ruptures or no rupture outside the nucleation region. There are no pulse-like ruptures. Representative cases separated by 0.5° in the inclination angle and marked by the small rectangles are analyzed further in Figs. 8 and 9

initiation procedure nucleates two healthy ruptures in the center of the interface, with almost identical sliding profiles (Fig. 8a, b). This is reasonable since the small difference in prestress is not sufficient to compete with the stress change due to the nucleation procedure. At a later time of 12 μs, the rupture has died out for the 23.5° case (Fig. 8c), but the rupture still exists for 24° case, albeit with smaller slip velocities (Fig. 8d). Clearly, in the case of 23.5°, rupture is unable to propagate outside of the nucleation region. At 20 μs, the interface continues to be locked for the case of 23.5° (Fig. 8e), while, for the case of 24°, the rupture is growing in comparison with the previous snapshot (Fig. 8f, d).

Slip evolution for the cases at the boundary between crack-like ruptures and no rupture propagation is presented in Fig. 9. Slip accumulation every 2 μs is shown. Results for the first parameter regime, already illustrated in Fig. 8, are given in the top row. There are only three lines for the case of 23.5°, which means that slip

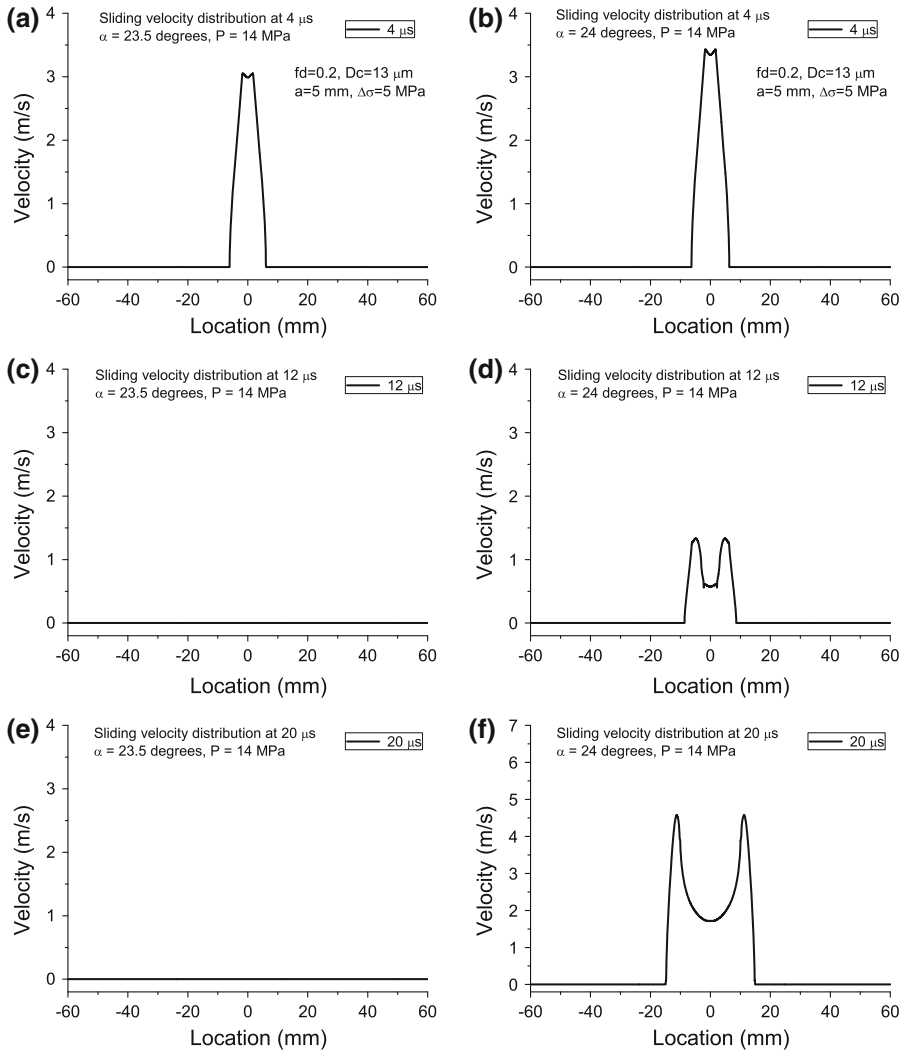

Fig. 8 Snapshots of sliding velocity for two simulations marked with *squares* in Fig. 7a. The *left column* shows a rupture that arrests right after the end of the nucleation process. The *right column* shows a crack-like rupture. The difference between the two cases is in the inclination angle, which is larger by 0.5° for the case on the *right*

arrests after about 6 μs, or right after the end of the nucleation procedure, which lasts 5 μs. The rupture is not able to propagate outside of the nucleation region that extends, for this parameter regime, 5 mm on both sides of the interface center. The case of 24° produces a healthy crack that transitions to supershear speeds. Results for the second parameter regime, with a much smaller critical slip distance of slip-weakening friction and hence a much smaller extend of the nucleation zone, from −0.8 mm to +0.8 mm, are shown in the bottom row. For the case of 24°, the nucleation procedure does not initiate sliding in the nucleation region, hence there is no rupture on the interface (Fig. 9c). For the case of slightly larger inclination angle of 24.5°, the numerical simulation results in a supershear crack (Fig. 9d).

These simulations suggest that the model with linear slip-weakening friction is unable to produce pulse-like ruptures, even in the presence of dynamic nucleation procedure that favors pulse-like ruptures due to its abruptness and short duration. Instead of rupture mode varying from crack-like to pulse-like with decreasing prestress, as observed in the experiments, simulations with linear slip weakening produce a direct change from no rupture propagation outside the nucleation region to crack-like rupture with a small increase in prestress. This is consistent with prior theoretical studies (Heaton 1990; Perrin et al. 1995; Zheng and Rice 1998) which found that slip-weakening friction is not sufficient to maintain pulse-like sliding, and velocity weakening of friction is required.

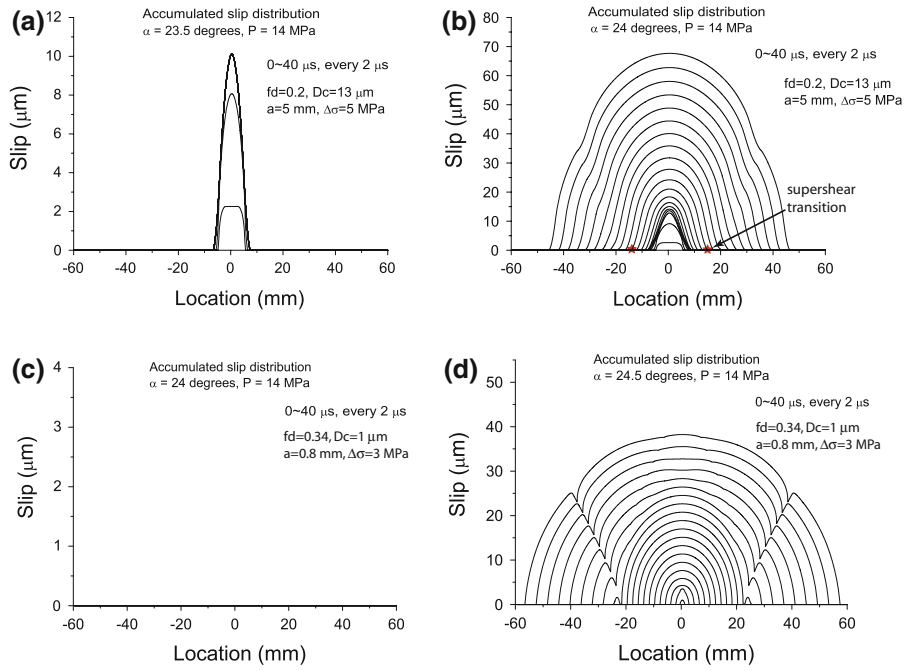

Fig. 9 Slip accumulation for the cases marked with *squares* in Fig. 7. **a–b** Two cases that represent change from no rupture to supershear crack-like rupture for the first parameter regime. **c–d** Two cases that represent change from no rupture to supershear crack-like rupture for the second parameter regime. For both (*a–b*) and (*c–d*), the two cases differ only by 0.5° in the inclination angle

4 Conclusions and discussion

Our experiments show that dynamic shear ruptures on interfaces prestressed in compression and in shear systematically vary from crack-like to pulse-like as the nondimensional shear prestress is reduced (Sect. 2; Lu et al. 2007, 2010). Similar systematic variation of rupture modes has also been observed for the decrease in absolute stress levels (Lu et al. 2010). Previous experimental studies have shown that both crack-like and pulse-like rupture modes can transition to supershear speeds, with pulse-like rupture modes having smaller supershear rupture speeds than crack-like modes (Lu et al. 2007, 2010). All of these experimental results are consistent with the theories of shear ruptures on velocity-weakening interfaces (Zheng and Rice 1998; Samudrala et al. 2002; Lu et al. 2007, 2010).

Our attempts to reproduce the systematic variation of rupture modes using the model with linear slip-weakening friction and a dynamic rupture initiation procedure have been unsuccessful (Sect. 3), despite the fact that Lu et al. (2009) were able to use the model to match supershear transition experiments of Xia et al. (2004). The simulations result either in crack-like ruptures or in ruptures that cannot propagate outside the nucleation region. Our numerical simulations suggest that interfaces governed by linear slip-weakening friction cannot produce pulse-like ruptures on homogeneous and uniformly prestressed interfaces even in the presence of a dynamic nucleation procedure. Note that it is still possible that some special choice of the nucleation procedure and parameters of linear slip weakening may result in transient pulse-like propagation outside of the nucleation region, as our simulations have not explored all parameter combinations; we have tested the parameter combinations that were shown to be potentially relevant to the experimental set up by Lu et al. (2010). However, the absence of even a single instance of pulse-like propagation in our simulations indicates the generic difficulty that the model has in reproducing pulse-like ruptures.

The experimental results and the simulations highlight the importance of velocity-weakening friction for shear rupture dynamics and the need to include velocity dependence of friction into earth -quake models. Our study implies that expressing dynamic weakening of friction solely in terms of slip may not be a sufficiently general description. An important future goal would be to measure the high-velocity friction properties of Homalite to check that its friction indeed exhibits velocity weakening as our study suggests.

Acknowledgments Nadia Lapusta gratefully acknowledges the support of NSF (Grant EAR 0548277) for this study. Ares J. Rosakis also gratefully acknowledges the support of NSF (Grant EAR 0207873), the US Department of Energy (Grant DE-FG52-06NA 26209) and MURI (Grant N000140610730, Dr. Y.D.S. Rajapakse, Program Manager). The numerical simulations for this research were performed on Caltech Division of Geological and Planetary Sciences Dell cluster.

References

Andrews DJ (1976) Rupture velocity of plane strain shear cracks. J Geophys Res 81:5679–5687

Andrews DJ, Ben-Zion Y (1997) Wrinkle-like slip pulse on a fault between different materials. J Geophys Res 102(B1):553–571

Archuleta RJ (1984) A faulting model for the 1979 Imperial-Valley earthquake. J Geophys Res 89(NB6):4559–4585

Beeler NM, Tullis TE (1996) Self-healing slip pulses in dynamic rupture models due to velocity-dependent strength. Bull Seismol Soc Am 86(4):1130–1148

Ben-Zion Y (2001) Dynamic ruptures in recent models of earthquake faults. J Mech Phys Solids 49(9):2209–2244

Beroza GC, Mikumo T (1996) Short slip duration in dynamic rupture in the presence of heterogeneous fault properties. J Geophys Res 101(B10):22449–22460

Cochard A, Madariaga R (1994) Dynamic faulting under rate-dependent friction. Pure Appl Geophys 142(3–4):419–445

Cochard A, Madariaga R (1996) Complexity of seismicity due to highly rate-dependent friction. J Geophys Res 101:25321–25336

Cochard A, Rice JR (2000) Fault rupture between dissimilar materials: ill-posedness, regularization, and slip-pulse response. J Geophys Res 105(B11):25891–25907

Dally JW, Riley WF (1991) Experimental stress analysis. McGraw-Hill, New York

Das SM, Aki K (1977) Numerical study of 2-dimensional spontaneous rupture propagation. Geophys J Royal Astro Soc 50(3):643–668

Day SM (1982) Three-dimensional finite difference simulation of fault dynamics: Rectangular faults with fixed rupture velocity. Bull Seismol Soc Am 72(3):705–727

Day SM, Yu G, Wald DJ (1998) Dynamic stress changes during earthquake rupture. Bull Seismol Soc Am 88(2):512–522

Di Toro G, Goldsby DL, Tullis TE (2004) Friction falls towards zero in quartz rock as slip velocity approaches seismic rates. Nature 427(6973):436–439

Dieterich JH (1979) Modeling of rock friction. 1. Experimental results and constitutive equations. J Geophys Res 84(NB5):2161–2168

Dieterich JH (1981) Constitutive properties of faults with simulated gouge. In: Carter NL et al. (eds) Mechanical behavior of crustal rocks, geophysical monograph. AGU, Washington, pp 103–120

Dieterich JH (2007) Application of rate- and state-dependent friction to models of fault slip and earthquake occurence. Treatise Geophys 4:107–129

Festa G, Vilotte JP (2006) Influence of the rupture initiation on the intersonic transition: crack-like versus pulse-like modes. Geophys Res Lett 33(15):L15320

Geubelle PH, Rice JR (1995) A spectral method for three-dimensional elastodynamic fracture problems. J Mech Phys Solids 43(11):1791–1824

Heaton TH (1990) Evidence for and implications of self-healing pulses of slip in earthquake rupture. Phys Earth Planet In 64(1):1–20

Ida Y (1972) Cohesive force across tip of a longitudinal-shear crack and Griffiths specific surface-energy. J Geophys Res 77(20):3796

Johnson E (1992) The influence of the lithospheric thickness on bilateral slip. Geophys J Int 108(1):151–160

Kanamori H, Anderson DL (1975) Theoretical basis of some empirical relations in seismology. Bull Seismol Soc Am 65(5):1073–1095

Kostrov BV (1966) Unsteady propagation of longitudinal shear cracks. J Appl Math Mech 30(6):1241

Lapusta N, Rice JR (2004) Earthquake sequences on rate and state faults with strong dynamic weakening. Eos Trans AGU 85(47):T22A–05

Liu Y, Lapusta N (2008) Transition of mode II cracks from sub-Rayleigh to intersonic speeds in the presence of favorable heterogeneity. J Mech Phys Solids 56(1):25–50

Lu X, Lapusta N, Rosakis AJ (2007) Pulse-like and crack-like ruptures in experiments mimicking crustal earthquakes. Proc Natl Acad Sci USA 104:18931–18936

Lu X, Lapusta N, Rosakis AJ (2009) Analysis of supershear transition regimes in rupture experiments: the effect of nucleation conditions and friction parameters. Geophys J Int 177(2):717–732

Lu X, Rosakis AJ, Lapusta N (2010) Rupture modes in laboratory earthquakes: effect of fault prestress and nucleation conditions. J Geophys Res

Lykotrafitis G, Rosakis AJ, Ravichandran G (2006a) Self-healing pulse-like shear ruptures in the laboratory. Science 313(5794):1765–1768

Lykotrafitis G, Rosakis AJ, Ravichandran G (2006b) Particle velocimetry and photoelasticity applied to the study of dynamic sliding along frictionally-held bimaterial interfaces: techniques and feasibility. Exp Mech 46(2):205–216

Madariaga R (1976) Dynamics of an expanding circular fault. Bull Seismol Soc Am 66(3):639–666

Madariaga R, Olsen KB (2000) Criticality of rupture dynamics in 3-D. Pure Appl Geophys 157:1981–2001

Nielsen SB, Carlson JM, Olsen KB (2000) Influence of friction and fault geometry on earthquake rupture. J Geophys Res 105(B3):6069–6088

Nielsen SB, Madariaga R (2003) On the self-healing fracture mode. Bull Seismol Soc Am 93(6):2375–2388

Noda H, Dunham EM, Rice JR (2009) Earthquake ruptures with thermal weakening and the operation of major faults at low overall stress levels. J Geophys Res. doi:10.1029/2008JB006143 (in press)

Olsen KB, Madariaga R, Archuleta RJ (1997) Three-dimensional dynamic simulation of the 1992 Landers earthquake. Science 278(5339):834–838

Perrin G, Rice JR, Zheng G (1995) Self-healing slip pulse on a frictional surface. J Mech Phys Solids 43(9):1461–1495

Rice JR (2006) Heating and weakening of faults during earthquake slip. J Geophys Res 111:B05311

Rosakis AJ (2002) Intersonic shear cracks and fault ruptures. Adv Phys 51:1189–1257

Rosakis AJ, Xia KW, Lykotrafitis G, Kanamori H (2007) Dynamic shear rupture in frictional interfaces: speeds, directionality and modes. In: Schubert G, Kanamori H (eds) Treatise in geophysics. Elsevier, Amsterdam

Ruina A (1983) Slip instability and state variable friction laws. J Geophys Res 88(NB12):359–370

Samudrala O, Huang Y, Rosakis AJ (2002) Subsonic and intersonic shear rupture of weak planes with a velocity weakening cohesive zone. J Geophys Res 107(B8):2170

Shi ZQ, Ben-Zion Y (2006) Dynamic rupture on a bimaterial interface governed by slip-weakening friction. Geophys J Int 165(2):469–484

Shi ZQ, Ben-Zion Y, Needleman A (2008) Properties of dynamic rupture and energy partition in a solid with a frictional interface. J Mech Phys Solids 56(1):5–24

Tsutsumi A, Shimamoto T (1997) High-velocity frictional properties of gabbro. Geophys Res Lett 24(6):699–702

Tullis TE (2007) Friction of rock at earthquake slip rates. In: Kanamori H (ed) Treatise on geophysics, vol 4. Elsevier, Amsterdam, 131–152

Tullis TE, Goldsby DL (2003) Flash melting of crustal rocks at almost seismic slip rates. Eos Trans AGU 84(46):S51B–05

Uenishi K, Rice JR (2003) Universal nucleation length for slip-weakening rupture instability under nonuniform fault loading. J Geophys Res 108(B1):2042

Xia KW, Rosakis AJ, Kanamori H (2004) Laboratory earthquakes: the Sub-rayleigh-to-supershear rupture transition. Science 303:1859–1861

Yuan F, Prakash V (2008a) Slip weakening in rocks and analog materials at co-seismic slip rates. J Mech Phys Sol 56:542–560

Yuan F, Prakash V (2008b) Use of a modified torsional Kolsky bar to study frictional slip resistance in rock-analog materials at coseismic slip rates. Int J Solids Struct 45:4247–4263

Zheng G, Rice JR (1998) Conditions under which velocity-weakening friction allows a self-healing versus a cracklike mode of rupture. Bull Seismol Soc Am 88:1466–1483